Cosmic radiation in the lower atmosphere with Airborne Gamma-Ray Spectroscopy

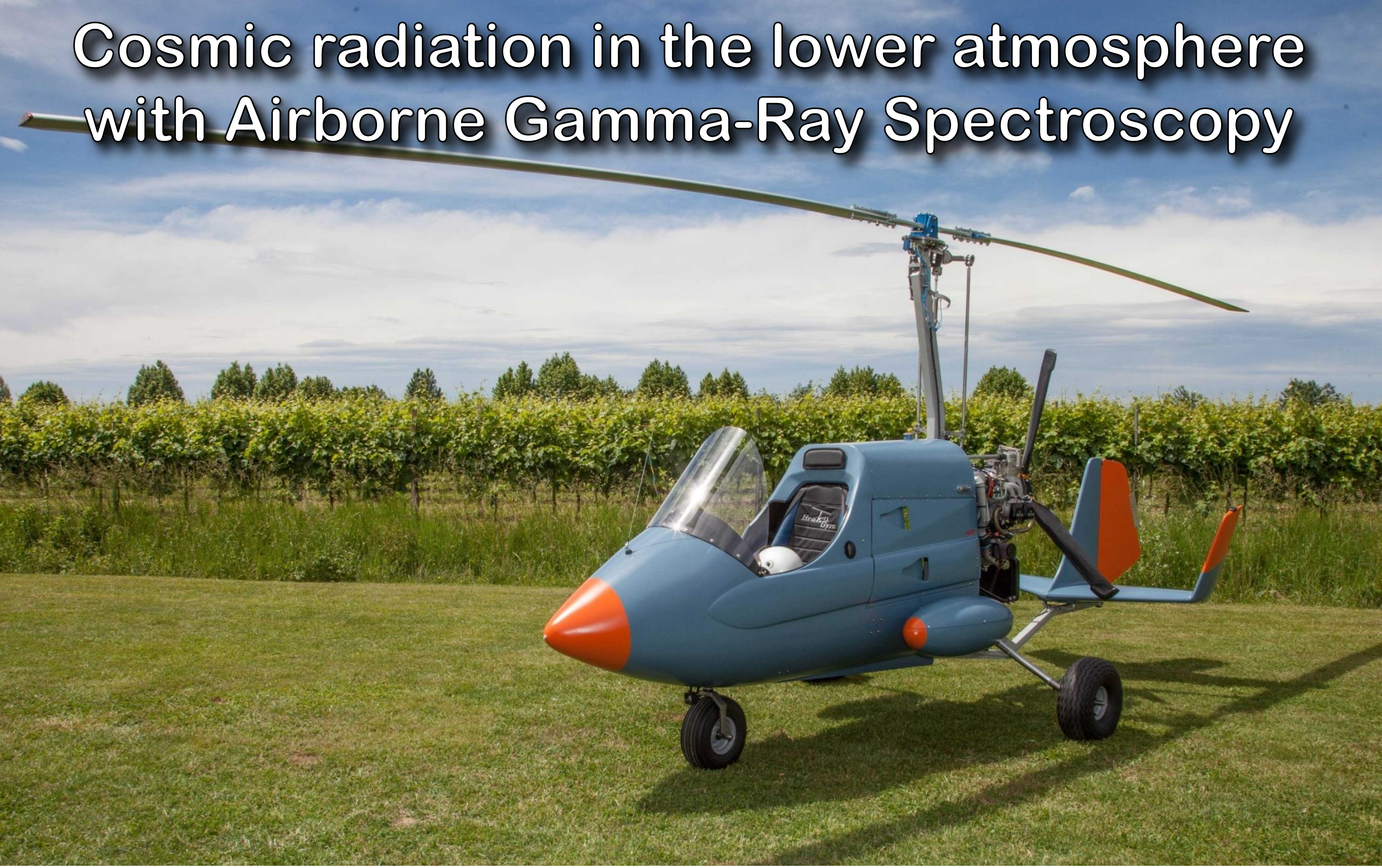

Marica Baldoncini

In collaboration with Matteo Albéri, Carlo Bottardi, Brian Minty, Kassandra Raptis, Virginia Strati and Fabio Mantovani

Università degli Studi di Ferrara

INFN Istituto Nazionale di Fisica Nucleare

European Geoscience Union General Assembly, 8 – 13 April 2018, Wien

Challenges in Airborne Gamma-Ray Spectroscopy (AGRS)

Challenges in Airborne Gamma-Ray Spectroscopy (AGRS)

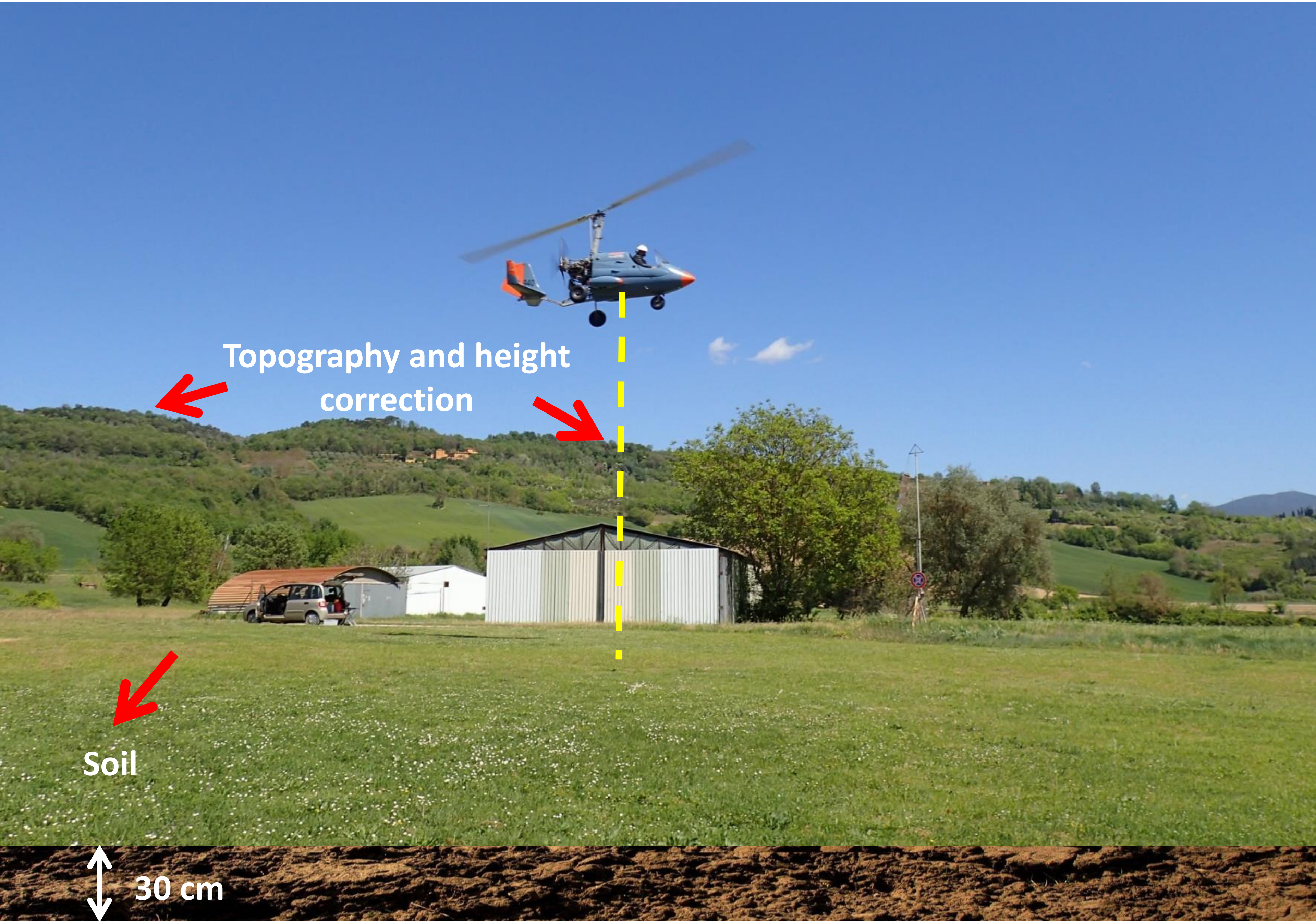

Challenges in Airborne Gamma-Ray Spectroscopy (AGRS)

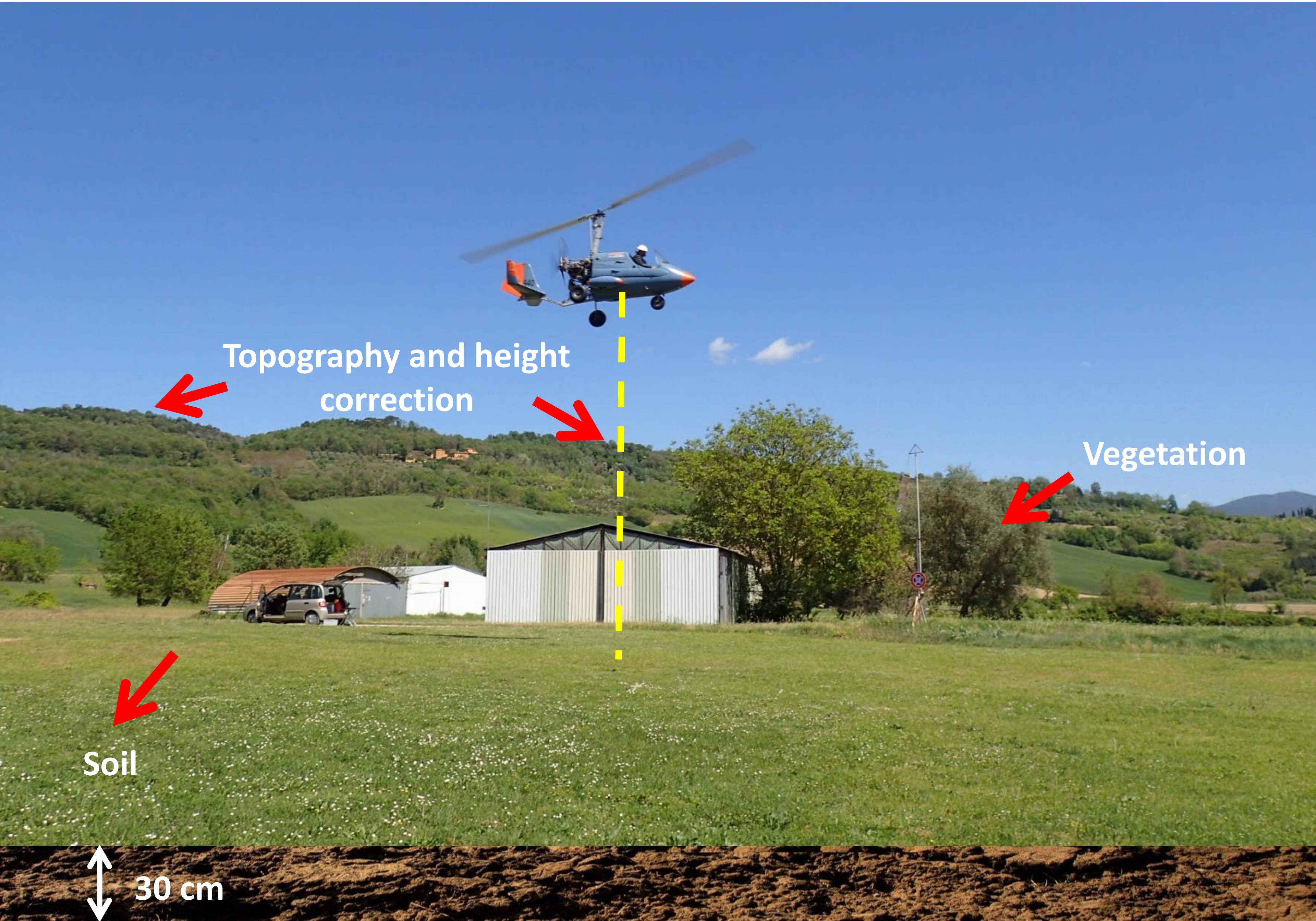

Challenges in Airborne Gamma-Ray Spectroscopy (AGRS)

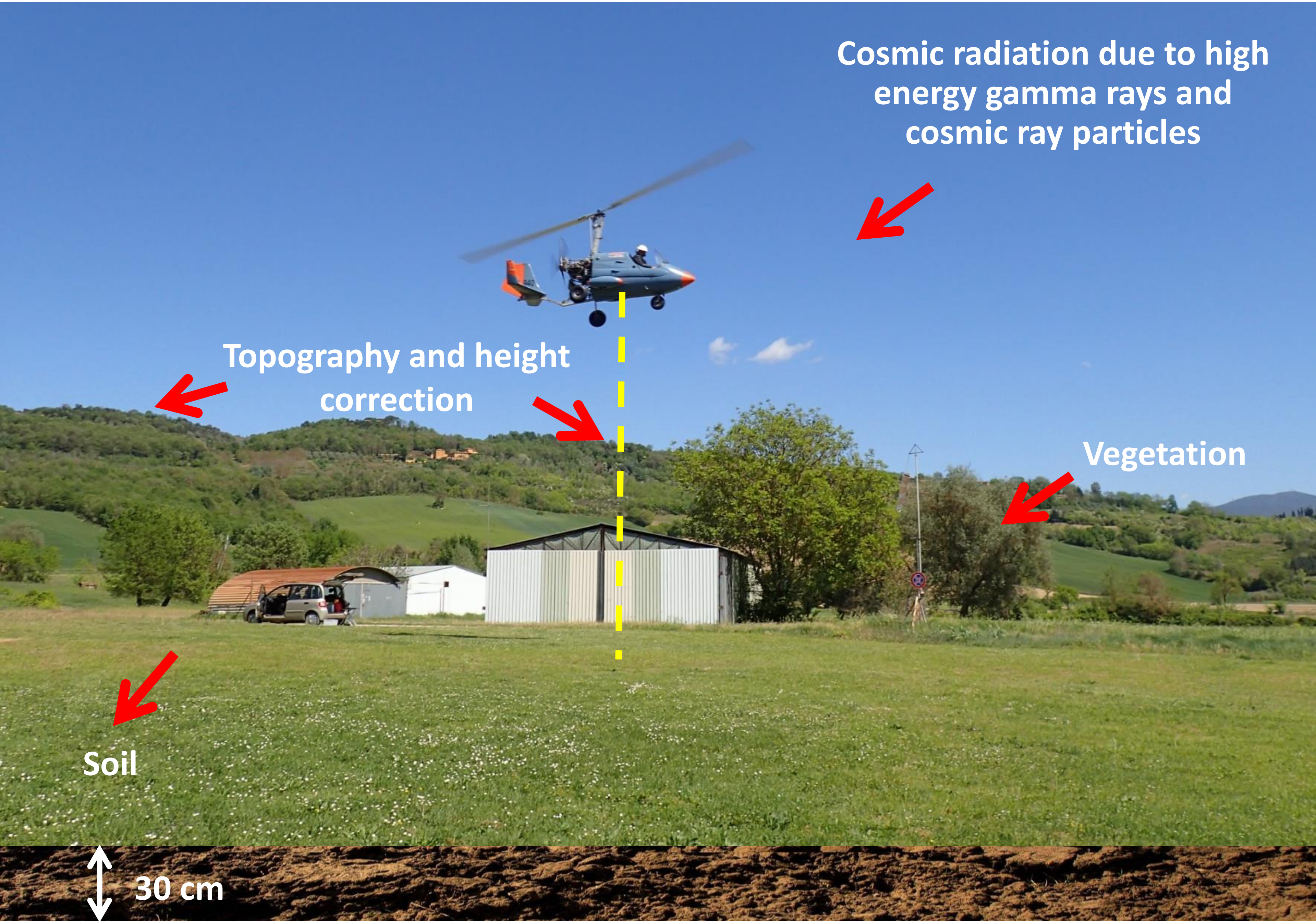

Challenges in Airborne Gamma-Ray Spectroscopy (AGRS)

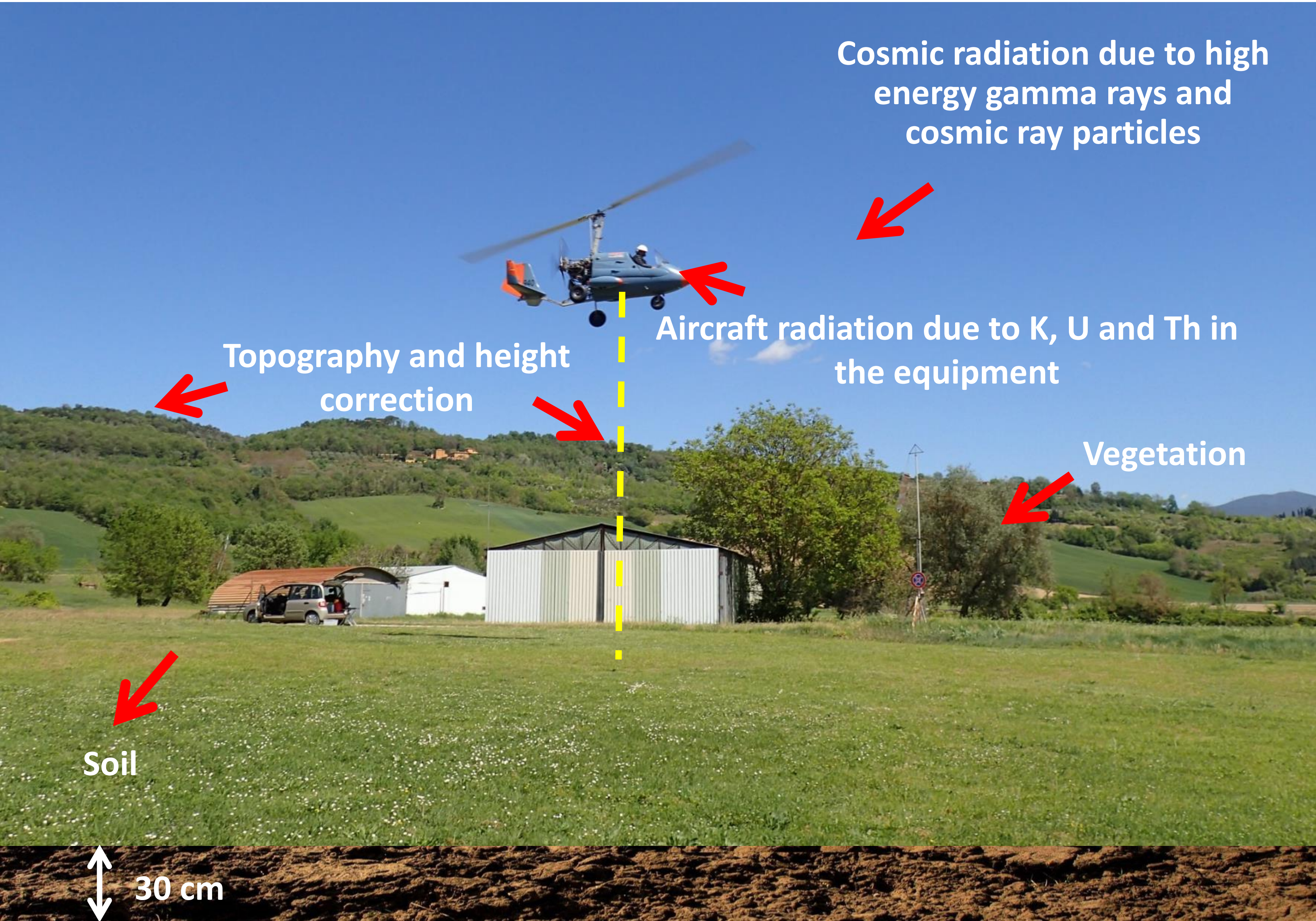

Challenges in Airborne Gamma-Ray Spectroscopy (AGRS)

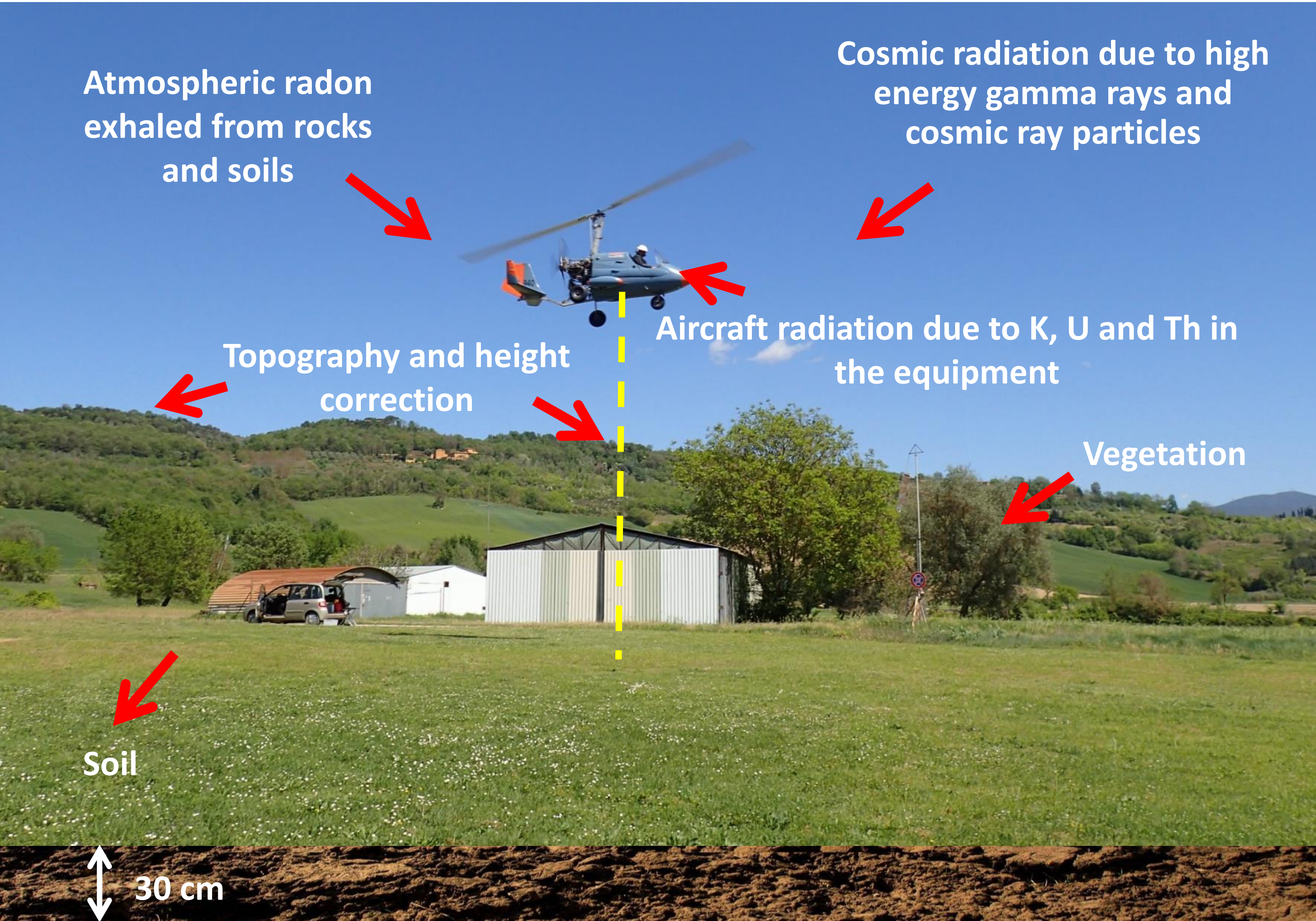

Challenges in Airborne Gamma-Ray Spectroscopy (AGRS)

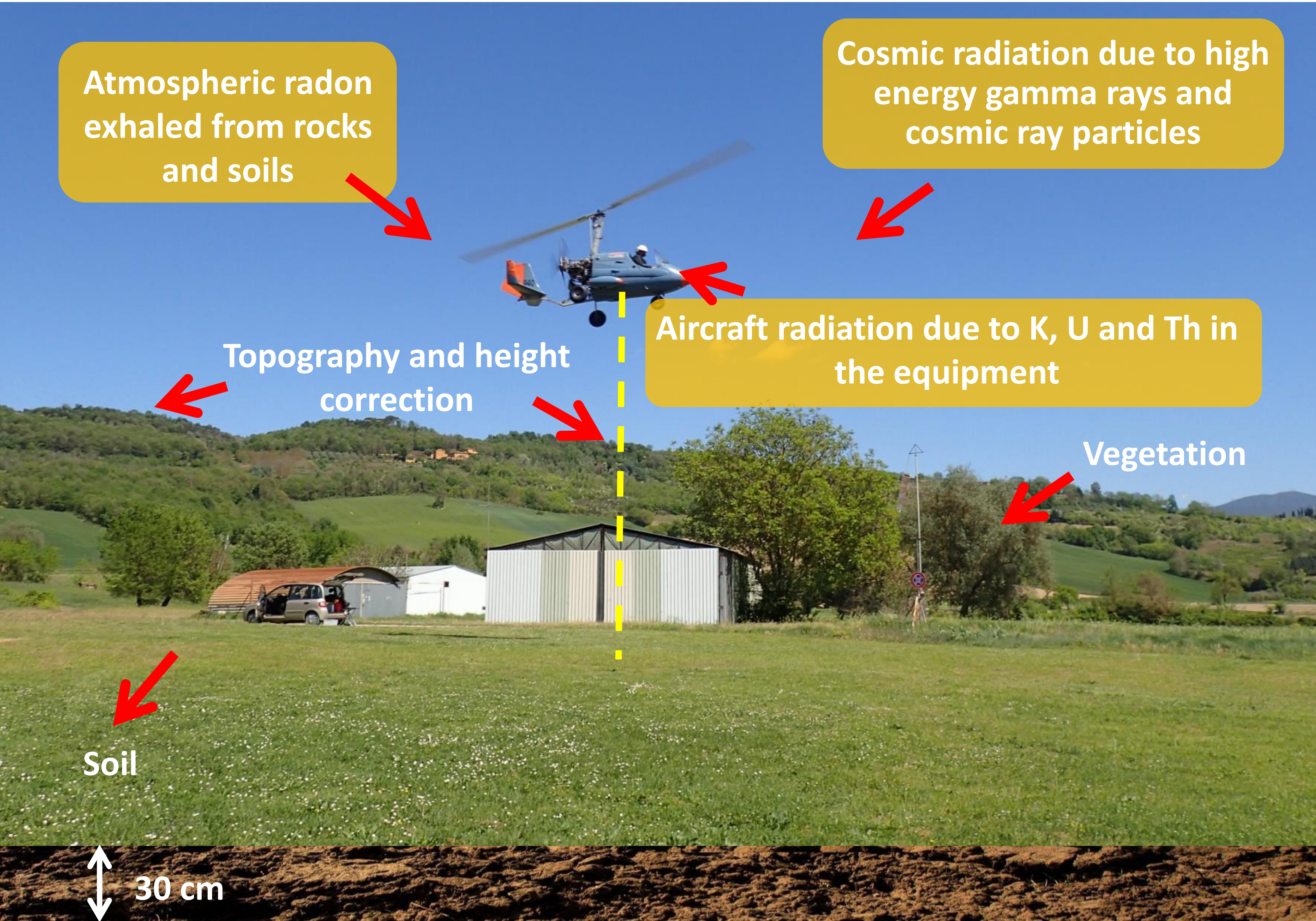

The Radgyro: a prototype aircraft for multiparametric surveys

- Engine: 1.6 liter turbo – 90 kW
- Payload: 150 kg
- Fuel: 90 liter of regular gasoline
- Length: 5.2 m
- Width: 2 m
- Rotor: 8.5 m
- Space for take off < 70 m
- Flight autonomy ~3.5 hours
- Investigated area ~50 km^2/h
- Easy to move without disassemble

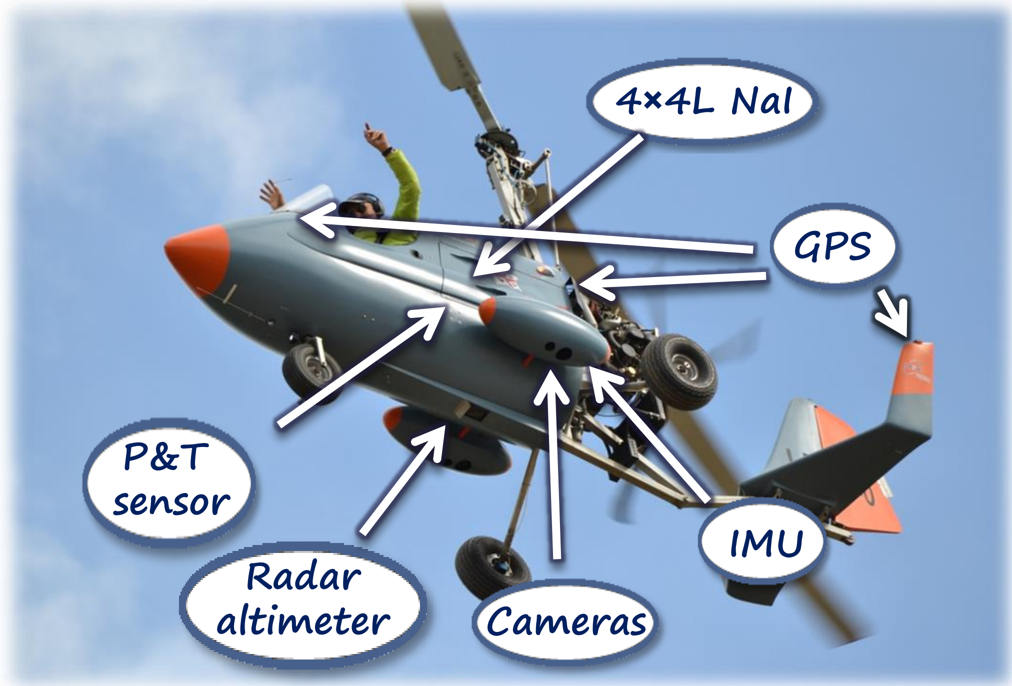

Offshore AGRS background calibration flights

4 offshore AGRS surveys for measuring the ***background*** due to:

- cosmic radiation
- experimental setup radioactivity
- ^{214}Bi coming from atmospheric ^{222}Rn

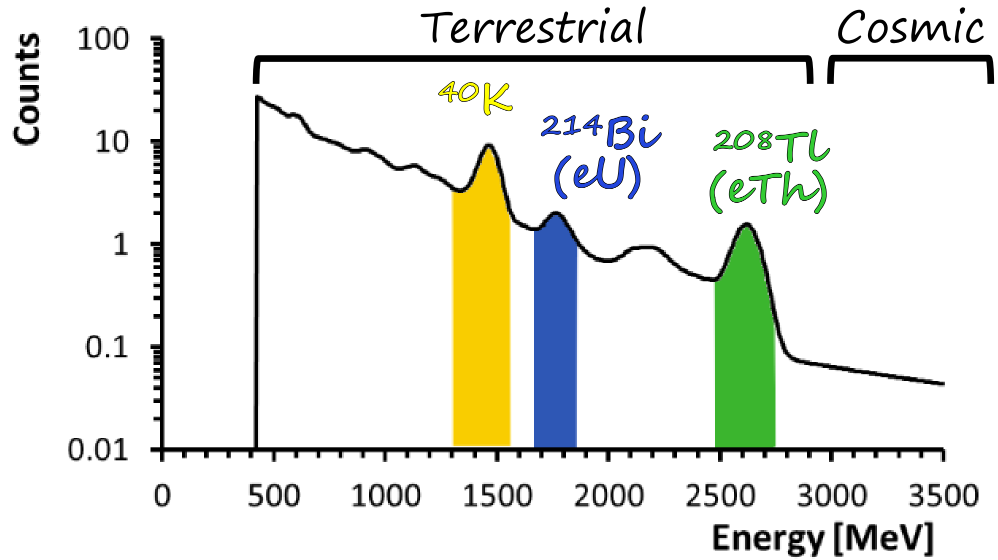

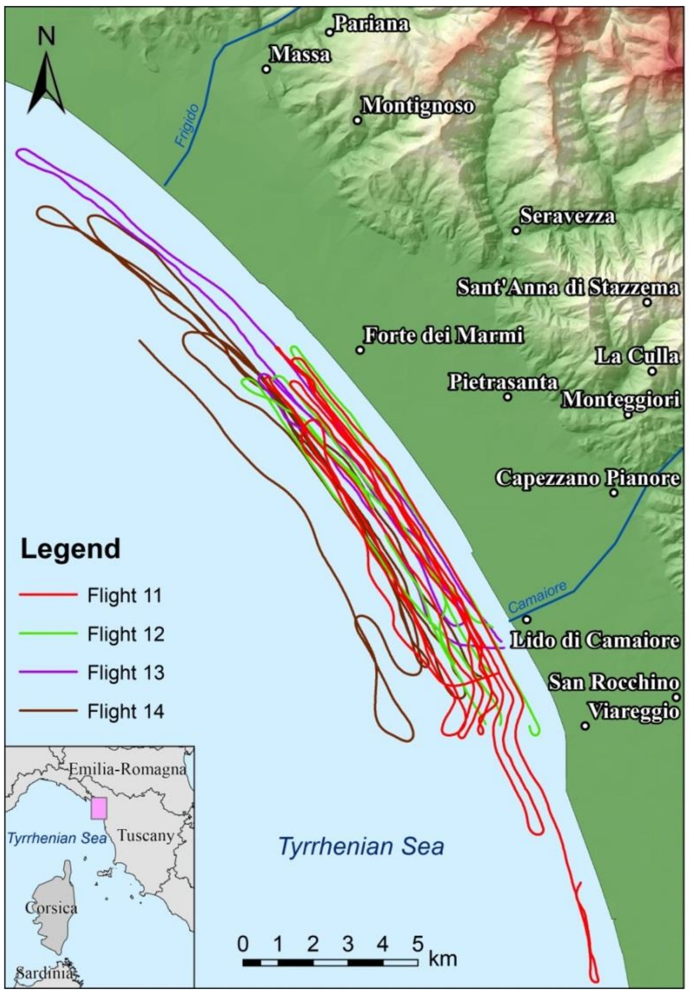

~5 hours of data taking over the sea in the (77 – 3066) m altitude range collecting ~17.6 10^3 spectra

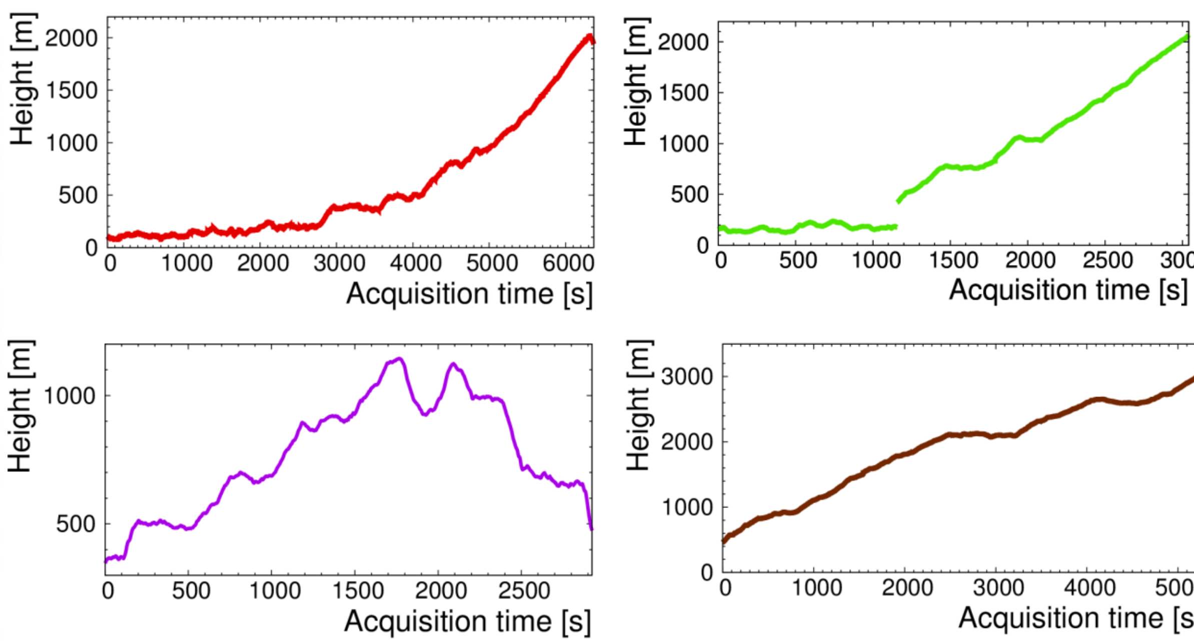

Count rate altitude profile

- Gamma cosmic radiation is a component of secondary cosmic rays
- At **E>3 MeV** all gamma radiation has **cosmic origin**
- In the lower atmosphere the intensity of cosmic gamma radiation **exponentially increases with increasing altitude:** the count rate altitude profile was reconstructed in the **Cosmic Energy Window (CEW)** (3.0 – 7.0) MeV and in the **Tallium Energy Window (TEW)** (2.4 – 2.8) MeV

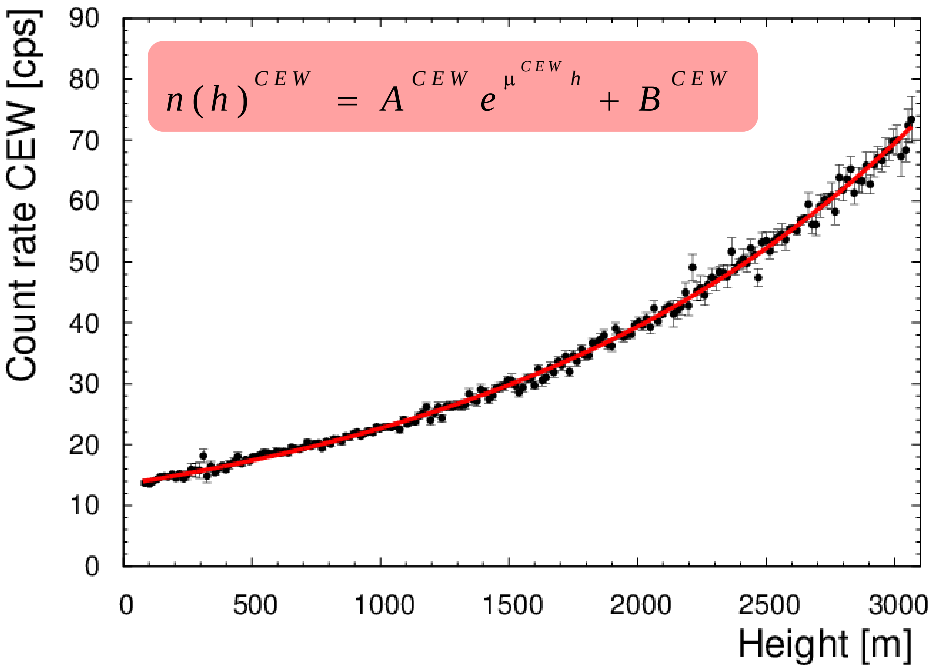

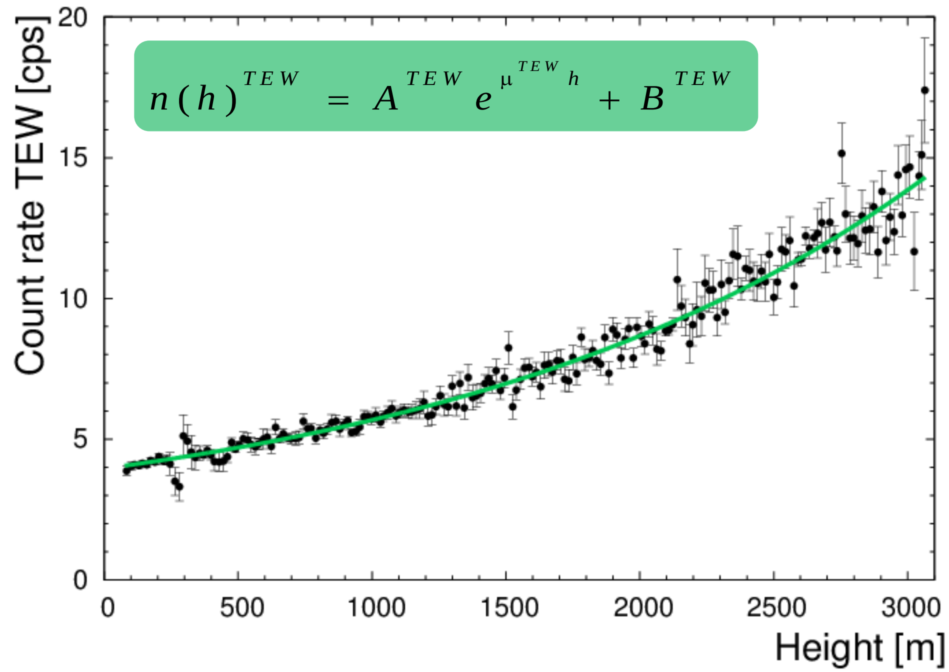

Energy Window	$(A \pm \delta A)$ [cps]	$(\mu \pm \delta\mu)$ [m^{-1}]	$(B \pm \delta B)$ [cps]	Reduced χ^2
CEW (3.0 – 7.0 MeV)	11.4 ± 0.3	$(5.9 \pm 0.1) \cdot 10^{-4}$	2.0 ± 0.4	1.12
TEW (2.4 – 2.8 MeV)	2.4 ± 0.2	$(5.5 \pm 0.2) \cdot 10^{-4}$	1.6 ± 0.2	0.94

Cosmic spectral shape

The cosmic spectral shape of a measured gamma spectrum can be reconstructed in the

- **Cosmic Energy Window (CEW)**: the counting statistics has pure cosmic nature but the sole reconstruction of the high energy tail is affected by large uncertainties

Gamma spectrum composed of 870 1 sec spectra acquired in the (2050 – 2150) m elevation range

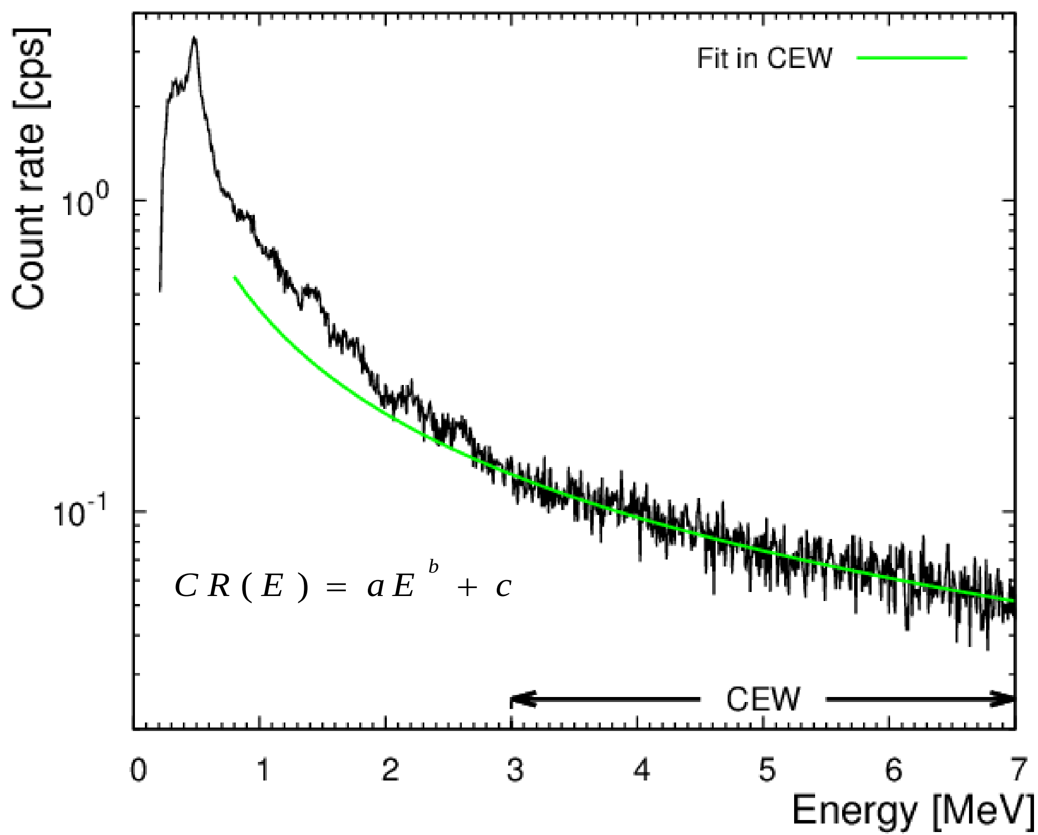

Energy Window	γ line [MeV]	Energy range [MeV]	Count rate at (2050 – 2150) m [cps]
KEW	1.46 (^{40}K)	1.37 – 1.57	12.2
BEW	1.76 (^{214}Bi)	1.66 – 1.86	8.7
TEW	2.61 (^{208}Tl)	2.41 – 2.81	8.8
CEW	/	3.00 – 7.00	41.9

Cosmic spectral shape

The cosmic spectral shape of a measured gamma spectrum can be reconstructed in the

- **Cosmic Energy Window (CEW)**: the counting statistics has pure cosmic nature but the sole reconstruction of the high energy tail is affected by large uncertainties
- **Full Energy Window (FEW)**: the measured count rates comprise not only the cosmic component, but also the signal coming from the **equipment radioactivity**

Gamma spectrum composed of 870 1 sec spectra acquired in the (2050 – 2150) m elevation range

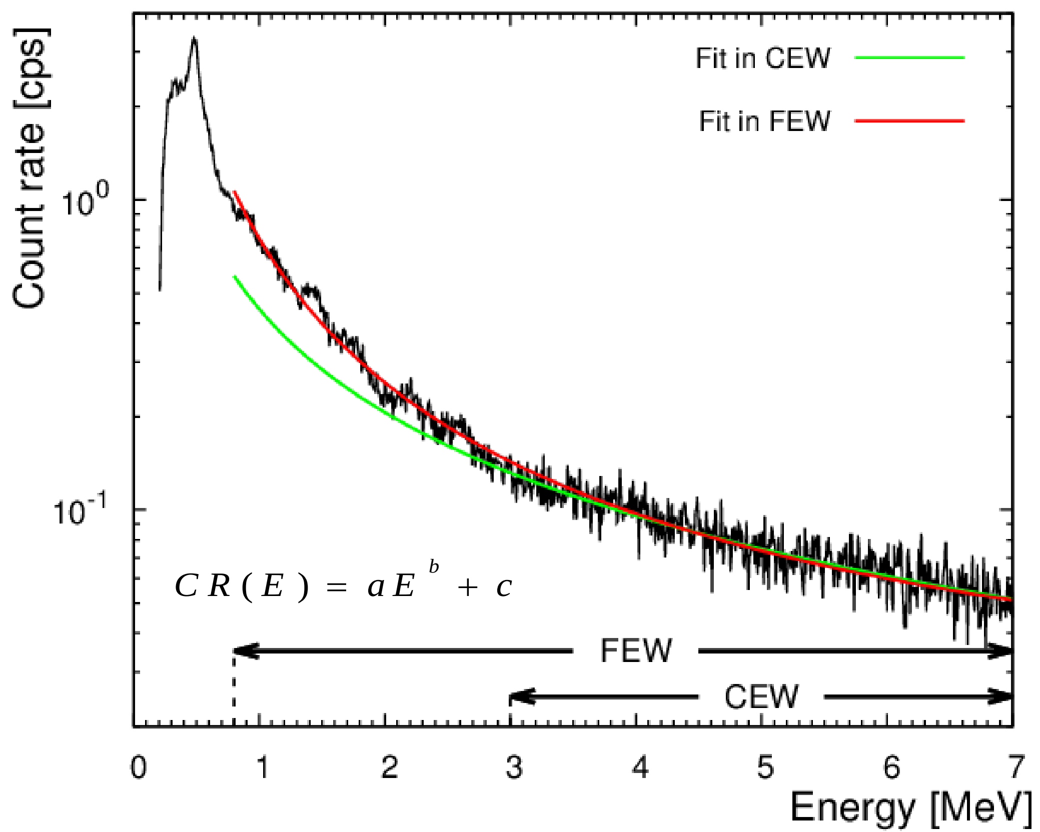

Energy Window	γ line [MeV]	Energy range [MeV]	Count rate at (2050 – 2150) m [cps]
KEW	1.46 (^{40}K)	1.37 – 1.57	12.2
BEW	1.76 (^{214}Bi)	1.66 – 1.86	8.7
TEW	2.61 (^{208}Tl)	2.41 – 2.81	8.8
CEW	/	3.00 – 7.00	41.9

Cosmic spectral shape

The cosmic spectral shape of a measured gamma spectrum can be reconstructed in the

- **Cosmic Energy Window (CEW)**: the counting statistics has pure cosmic nature but the sole reconstruction of the high energy tail is affected by large uncertainties
- **Full Energy Window (FEW)**: the measured count rates comprise not only the cosmic component, but also the signal coming from the **equipment radioactivity**
- **CEW + ^{40}K + ^{214}Bi + ^{208}Tl photopeaks** aid constraining the low energy trend of the cosmic shape, necessary to separate the constant count rate components due to **K, U and Th in the equipment**

Gamma spectrum composed of 870 1 sec spectra acquired in the (2050 – 2150) m elevation range

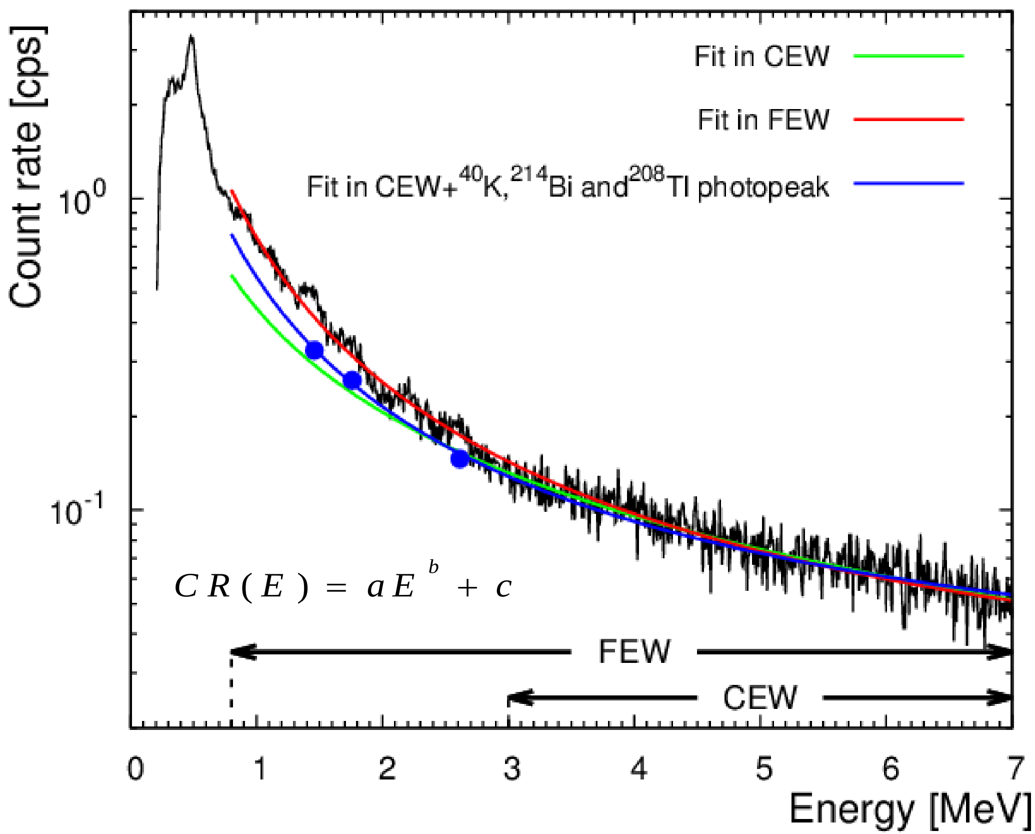

Energy Window	γ line [MeV]	Energy range [MeV]	Count rate at (2050 – 2150) m [cps]
KEW	1.46 (^{40}K)	1.37 – 1.57	12.2
BEW	1.76 (^{214}Bi)	1.66 – 1.86	8.7
TEW	2.61 (^{208}Tl)	2.41 – 2.81	8.8
CEW	/	3.00 – 7.00	41.9

Cosmic and aircraft background count rates

The CR in the natural radionuclides energy windows are linearly related to the count rate in the CEW

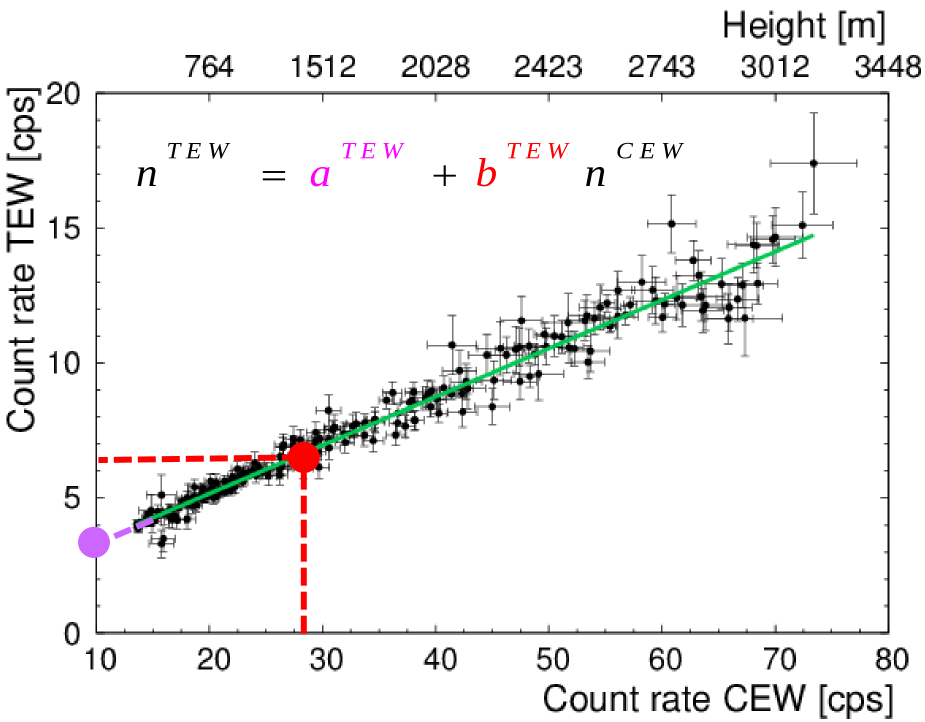

Linear regressions between count rates in the *i-th* energy window and in CEW allow for correcting for background the CRs measured during regional AGRS surveys

b: cosmic stripping ratio

a: aircraft constant background count rate

Energy Window	(a ± δa) [cps]	(b ± δb) [cps/cps in CEW]	MDA	Reduced χ2
KEW	3.7 ± 0.4	0.20 ± 0.01	$0.05 \cdot 10^{-2}$ g/g	1.00
BEW	2.0 ± 0.4	0.16 ± 0.01	0.4 µg/g	1.02
TEW	1.58 ± 0.04	0.179 ± 0.002	0.8 µg/g	1.02

Cosmic and aircraft background count rates

The CR in the natural radionuclides energy windows are linearly related to the count rate in the CEW

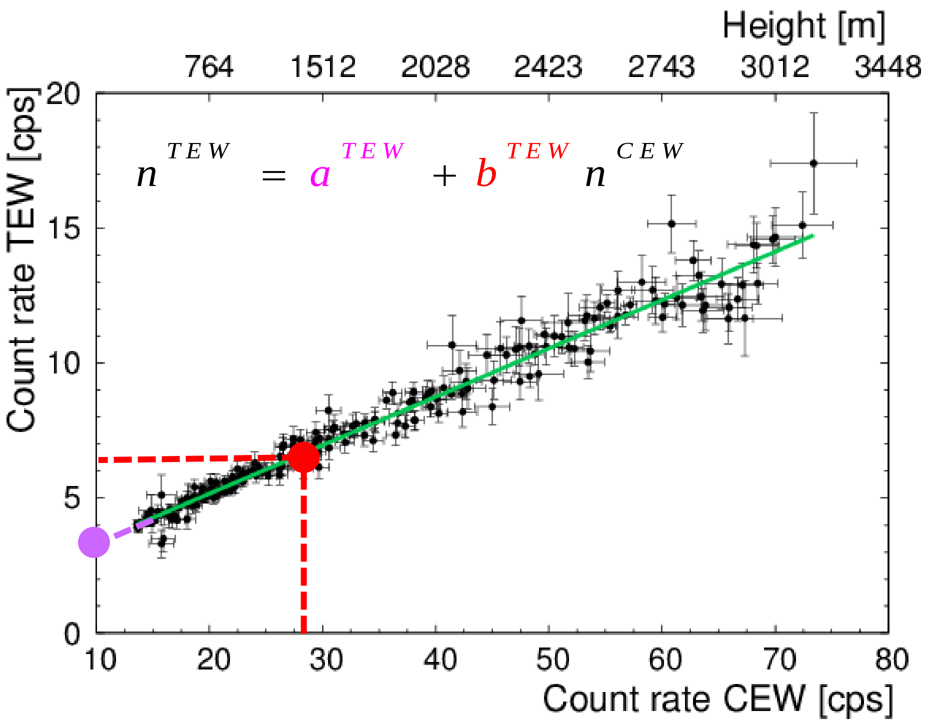

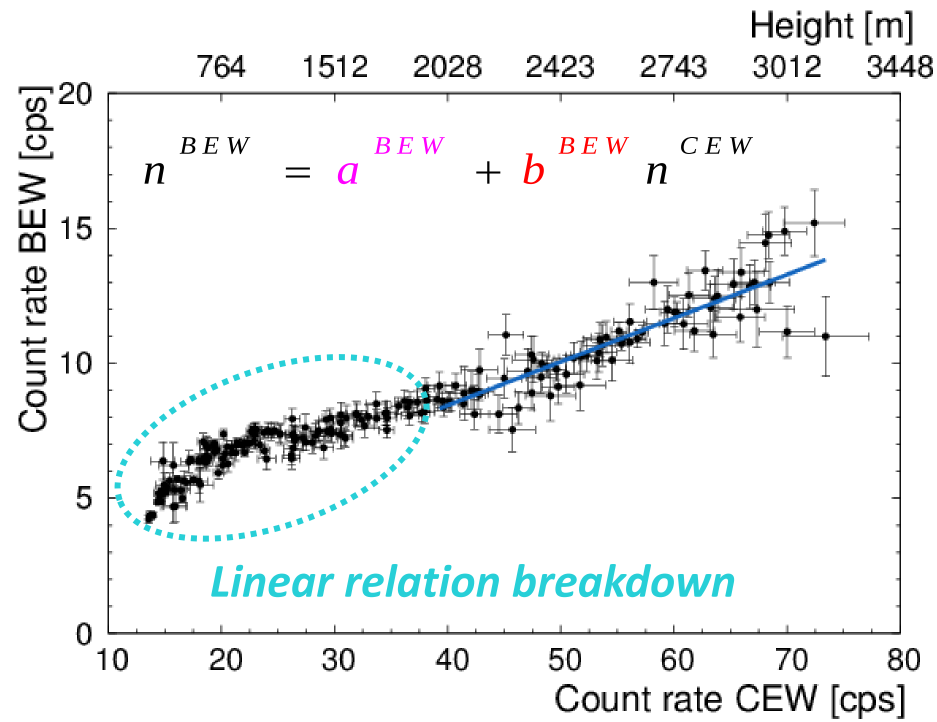

Linear regressions between count rates in the *i-th* energy window and in CEW allow for correcting for background the CRs measured during regional AGRS surveys

b: cosmic stripping ratio

a: aircraft constant background count rate

Energy Window	(a ± δa) [cps]	(b ± δb) [cps/cps in CEW]	MDA	Reduced χ2
KEW	3.7 ± 0.4	0.20 ± 0.01	$0.05 \cdot 10^{-2}$ g/g	1.00
BEW	2.0 ± 0.4	0.16 ± 0.01	0.4 μg/g	1.02
TEW	1.58 ± 0.04	0.179 ± 0.002	0.8 μg/g	1.02

A new model for the BEW count rate altitude profile

- In presence of atmospheric radon, the CR in the BEW comprises an additional altitude dependent component coming from atmospheric ^{214}Bi (Rn):

$$n(h) = A^{BEW} e^{\mu^{BEW} h} + B^{BEW} + n_{Rn}$$

- Atmospheric ^{222}Rn vertical profile typically shows a diurnal mixing layer at s ~ 1-2 km
- A new theoretical model was developed to describe the n_{Rn} vertical profile on the basis of the ^{222}Rn concentration distribution and of the mean free path of ^{214}Bi unscattered photons, which is responsible for the r ~ 400 m AGRS spherical field of view

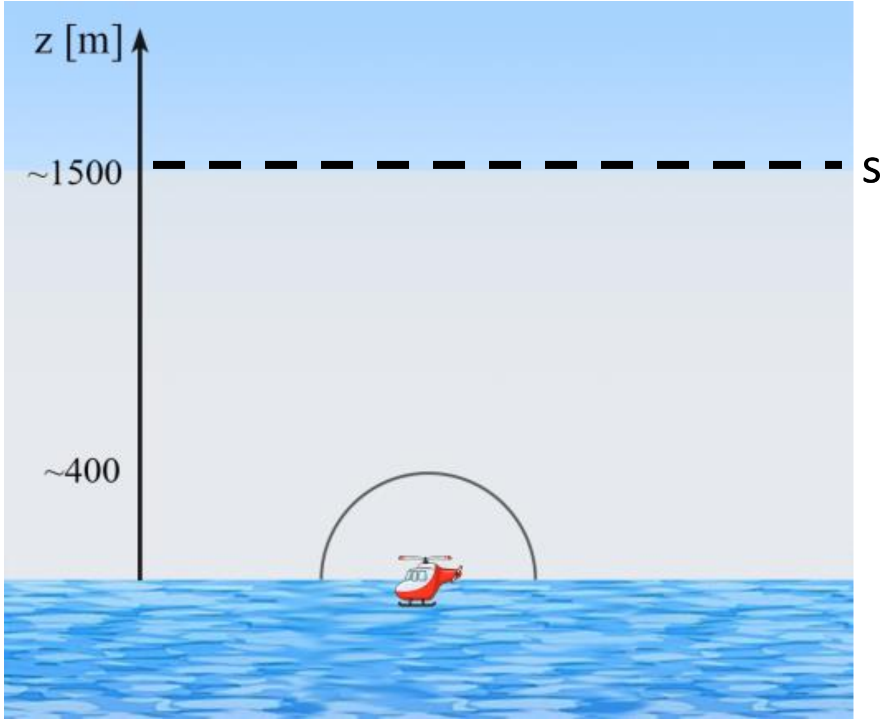

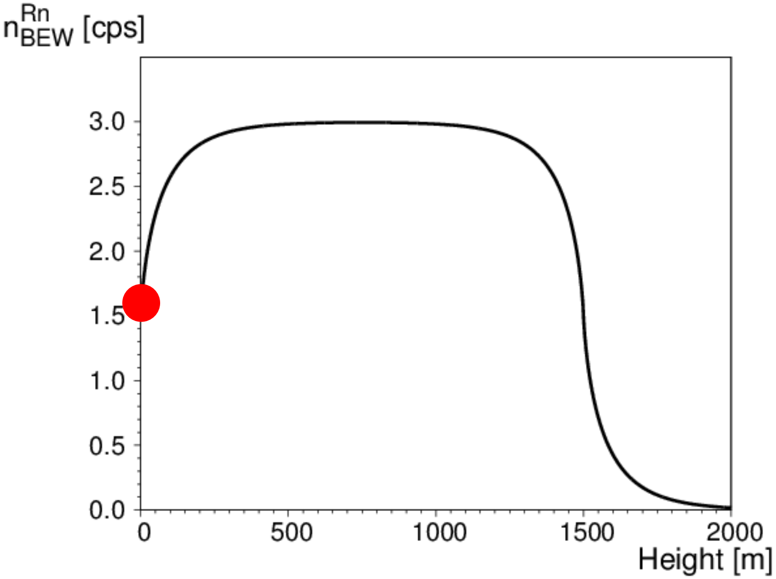

A new model for the BEW count rate altitude profile

- In presence of atmospheric radon, the CR in the BEW comprises an additional altitude dependent component coming from atmospheric ^{214}Bi (Rn):

$$n(h) = A^{BEW} e^{\mu^{BEW} h} + B^{BEW} + n_{Rn}$$

- Atmospheric ^{222}Rn vertical profile typically shows a diurnal mixing layer at s ~ 1-2 km

- A new theoretical model was developed to describe the n_{Rn} vertical profile on the basis of the ^{222}Rn concentration distribution and of the mean free path of ^{214}Bi unscattered photons, which is responsible for the r ~ 400 m AGRS spherical field of view

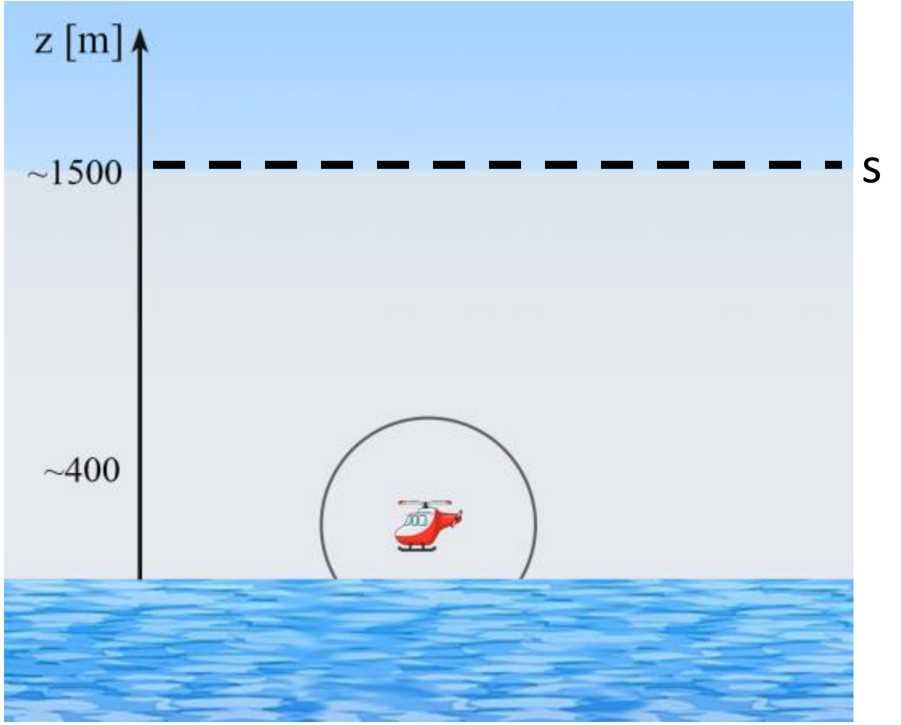

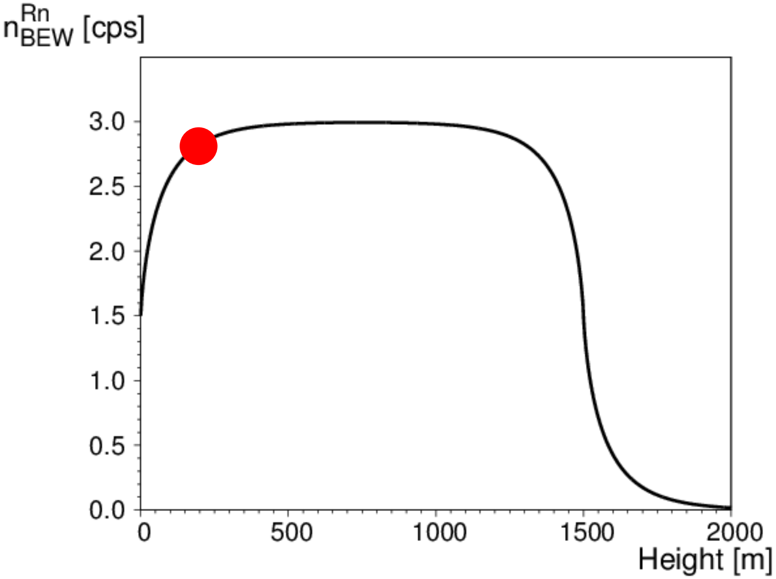

A new model for the BEW count rate altitude profile

- In presence of atmospheric radon, the CR in the BEW comprises an additional altitude dependent component coming from atmospheric ^{214}Bi (Rn):

$$n(h) = A^{BEW} e^{\mu^{BEW} h} + B^{BEW} + n_{Rn}$$

- Atmospheric ^{222}Rn vertical profile typically shows a diurnal mixing layer at s ~ 1-2 km

- A new theoretical model was developed to describe the n_{Rn} vertical profile on the basis of the ^{222}Rn concentration distribution and of the mean free path of ^{214}Bi unscattered photons, which is responsible for the r ~ 400 m AGRS spherical field of view

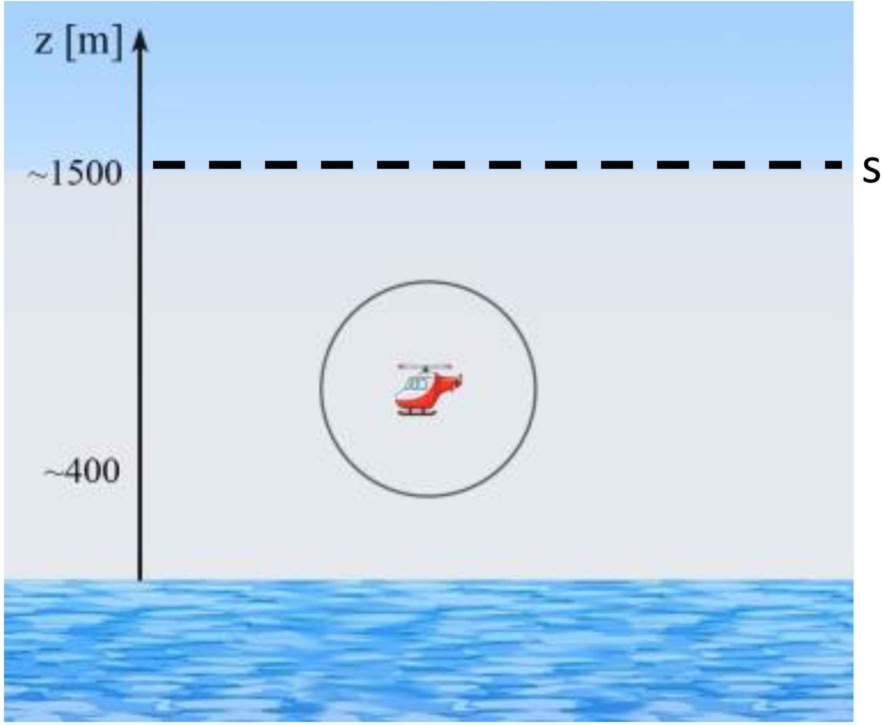

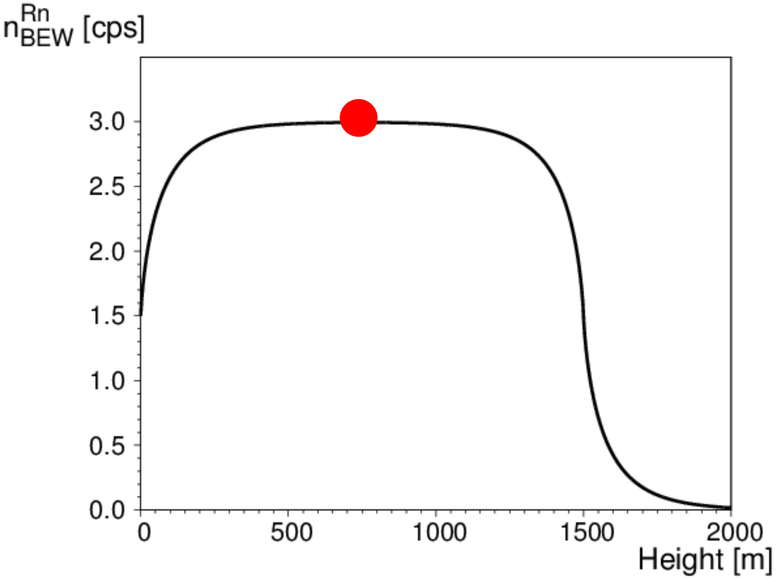

A new model for the BEW count rate altitude profile

- In presence of atmospheric radon, the CR in the BEW comprises an additional altitude dependent component coming from atmospheric ^{214}Bi (Rn):

$$n(h) = A^{BEW} e^{\mu^{BEW} h} + B^{BEW} + n_{Rn}$$

- Atmospheric ^{222}Rn vertical profile typically shows a diurnal mixing layer at s ~ 1-2 km
- A new theoretical model was developed to describe the n_{Rn} vertical profile on the basis of the ^{222}Rn concentration distribution and of the mean free path of ^{214}Bi unscattered photons, which is responsible for the r ~ 400 m AGRS spherical field of view

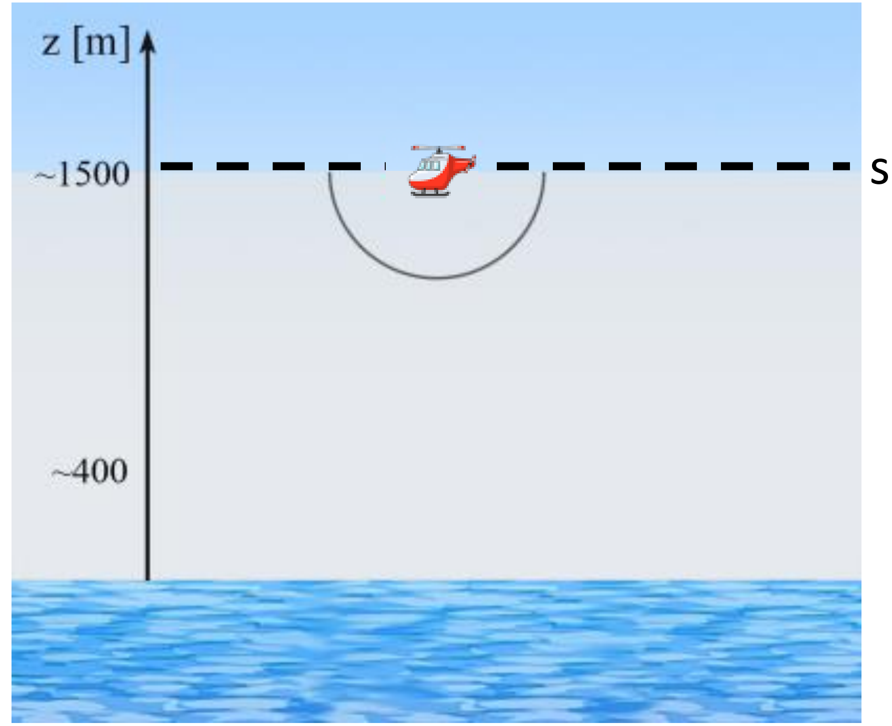

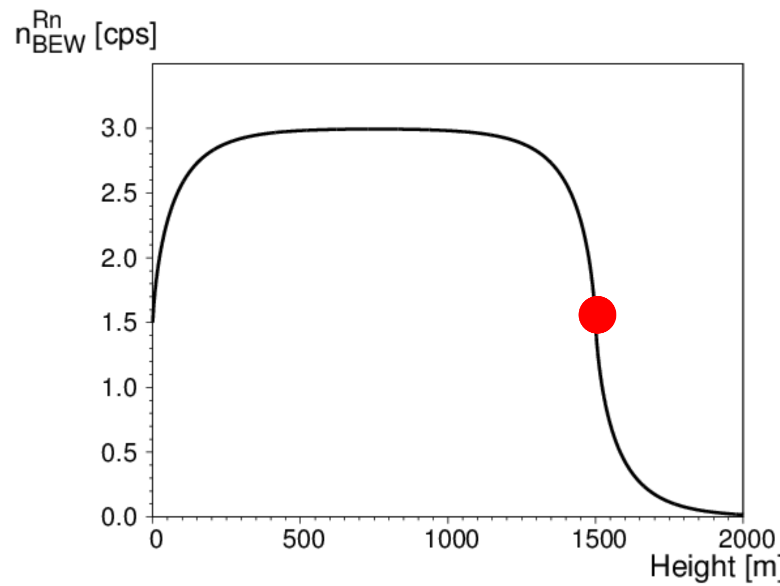

A new model for the BEW count rate altitude profile

- In presence of atmospheric radon, the CR in the BEW comprises an additional altitude dependent component coming from atmospheric ^{214}Bi (Rn):

$$n(h) = A^{BEW} e^{\mu^{BEW} h} + B^{BEW} + n_{Rn}$$

- Atmospheric ^{222}Rn vertical profile typically shows a diurnal mixing layer at s ~ 1-2 km
- A new theoretical model was developed to describe the n_{Rn} vertical profile on the basis of the ^{222}Rn concentration distribution and of the mean free path of ^{214}Bi unscattered photons, which is responsible for the r ~ 400 m AGRS spherical field of view

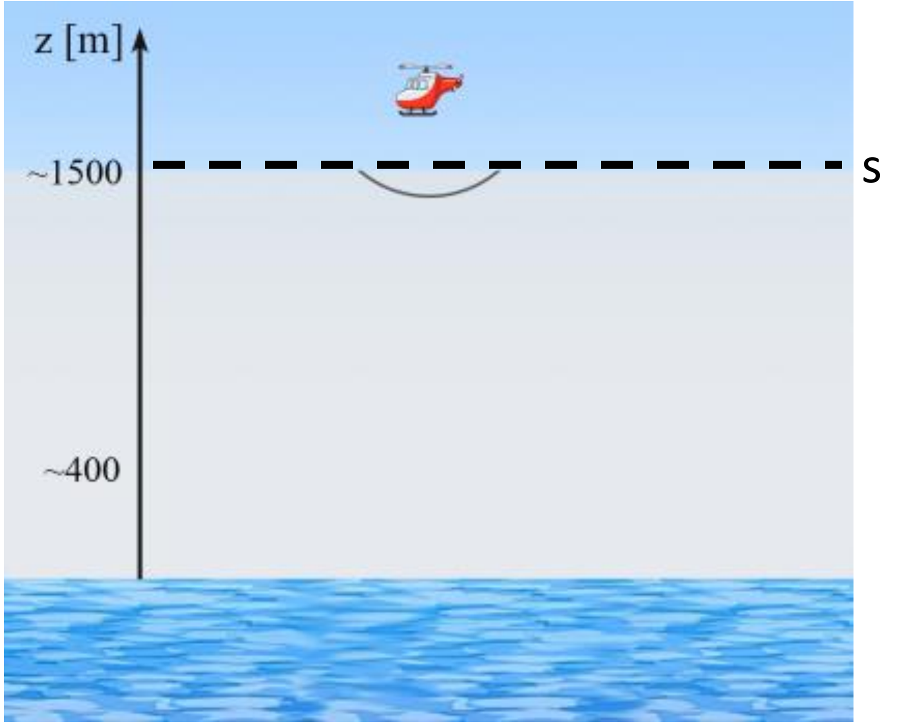

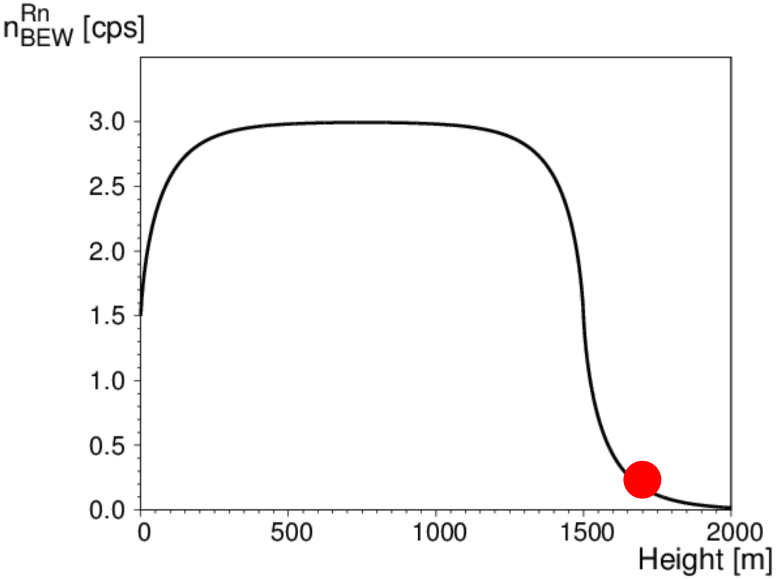

A new model for the BEW count rate altitude profile

- In presence of atmospheric radon, the CR in the BEW comprises an additional altitude dependent component coming from atmospheric ^{214}Bi (Rn):

$$n(h) = A^{BEW} e^{\mu^{BEW} h} + B^{BEW} + n_{Rn}$$

- Atmospheric ^{222}Rn vertical profile typically shows a diurnal mixing layer at s ~ 1-2 km

- A new theoretical model was developed to describe the n_{Rn} vertical profile on the basis of the ^{222}Rn concentration distribution and of the mean free path of ^{214}Bi unscattered photons, which is responsible for the r ~ 400 m AGRS spherical field of view

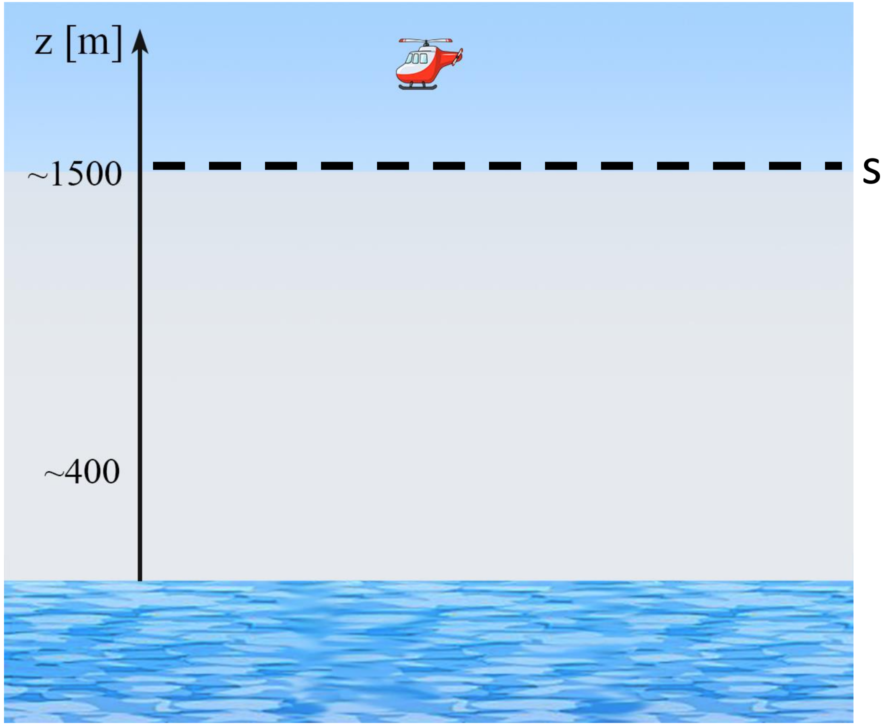

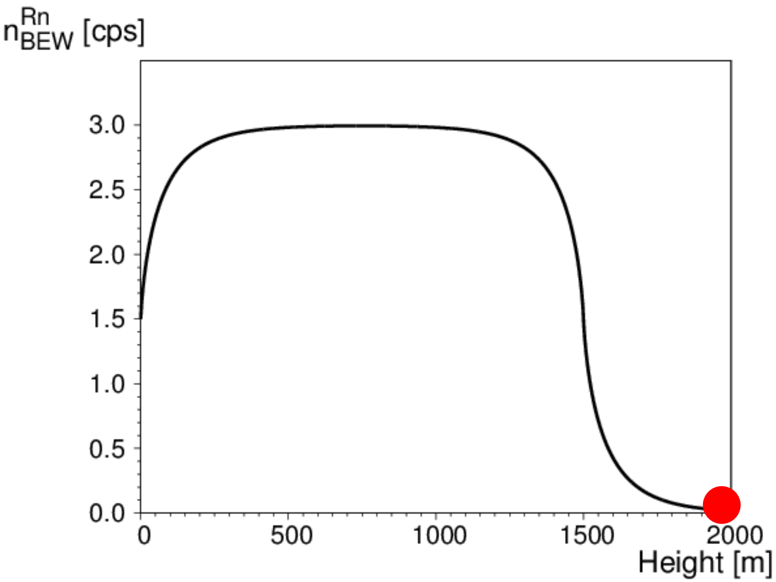

Full reconstruction of the BEW count rate altitude profile

The theoretical model is applied for fitting the experimental count rate in the BEW

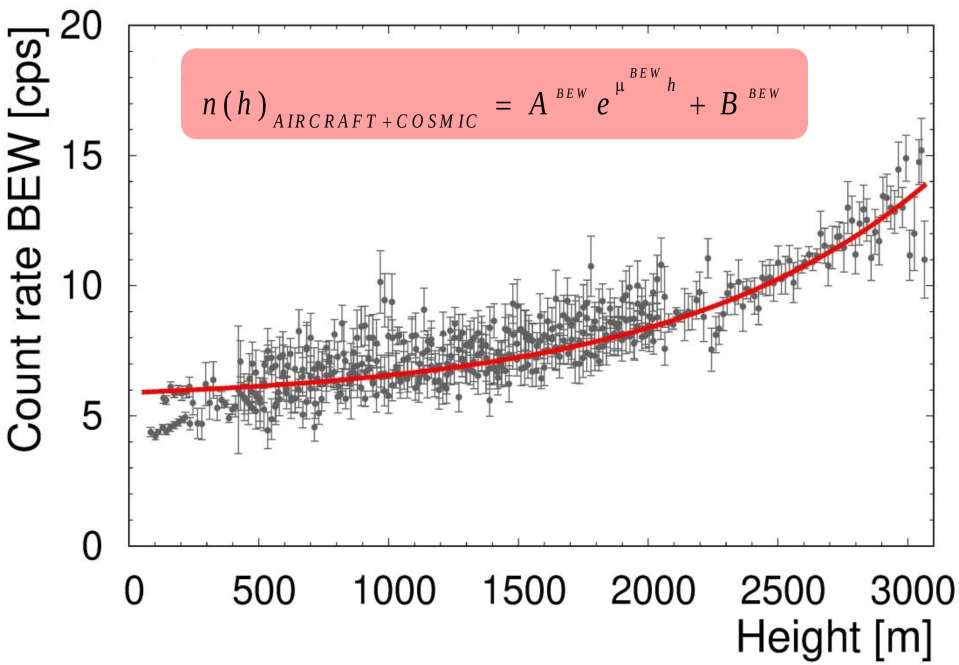

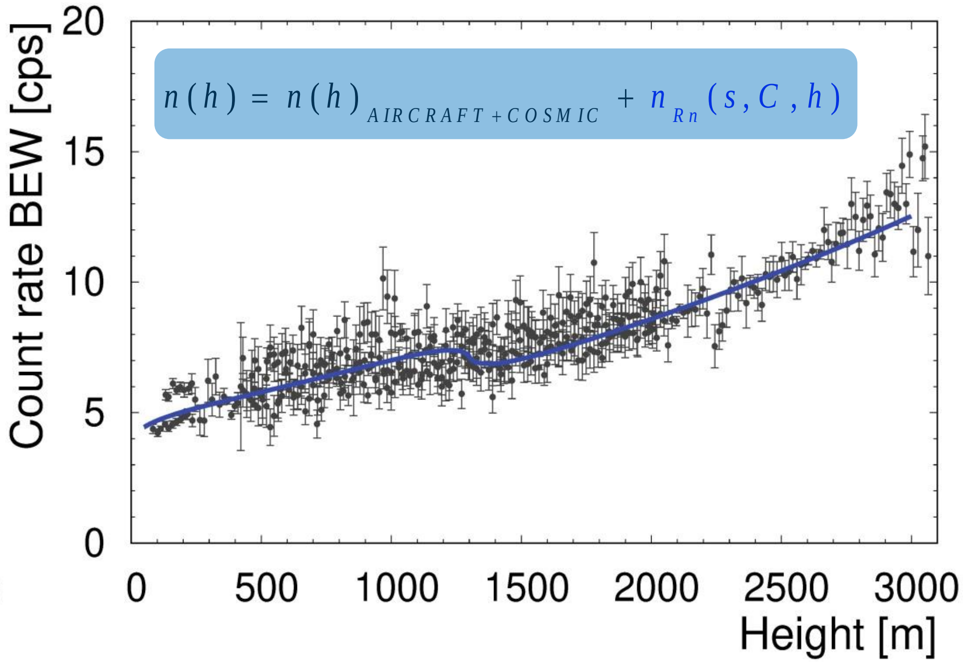

Model	$A_{BEW} \pm \delta A_{BEW}$ [cps]	$\mu_{BEW} \pm \delta\mu_{BEW}$ [m^{-1}]	$B_{BEW} \pm \delta B_{BEW}$ [cps]	$s \pm \delta s$ [m]	$C \pm \delta C$ [cps]	Reduced χ^2
Standard model	0.39 ± 0.07	$(2.01 \pm 0.1) \cdot 10^{-3}$	5.5 ± 0.3	/	/	**5.0**
New model	8.2 ± 0.2	$(2.54 \pm 0.06) \cdot 10^{-4}$	-4.9 ± 0.2	1318 ± 22	0.68 ± 0.05	**2.1**

- The **new model**, accounting for the a **homogeneous ^{222}Rn layer**, provides a better fit compared to the **^{222}Rn free standard model**
- The mean ^{222}Rn concentration **a_{Rn} = (0.96± 0.07) Bq/m^3** and mixing layer depth **s = (1322 ± 22)** m are in agreement with the literature

See Poster "Atmospheric Radon in a marine environment: a novel approach based on AGRS" X4.307 17.30 – 19.00

AGRS for measuring cosmic effective dose

- The AGRS detector was calibrated for the ElectroMagnetic Shower component of the cosmic effective dose (CED^{EMS}) by means of the **CARI-6P** and **EXPACS** dosimetry software tools
- On the basis of this calibration, the AGRS spectrometer can be used a dosimeter

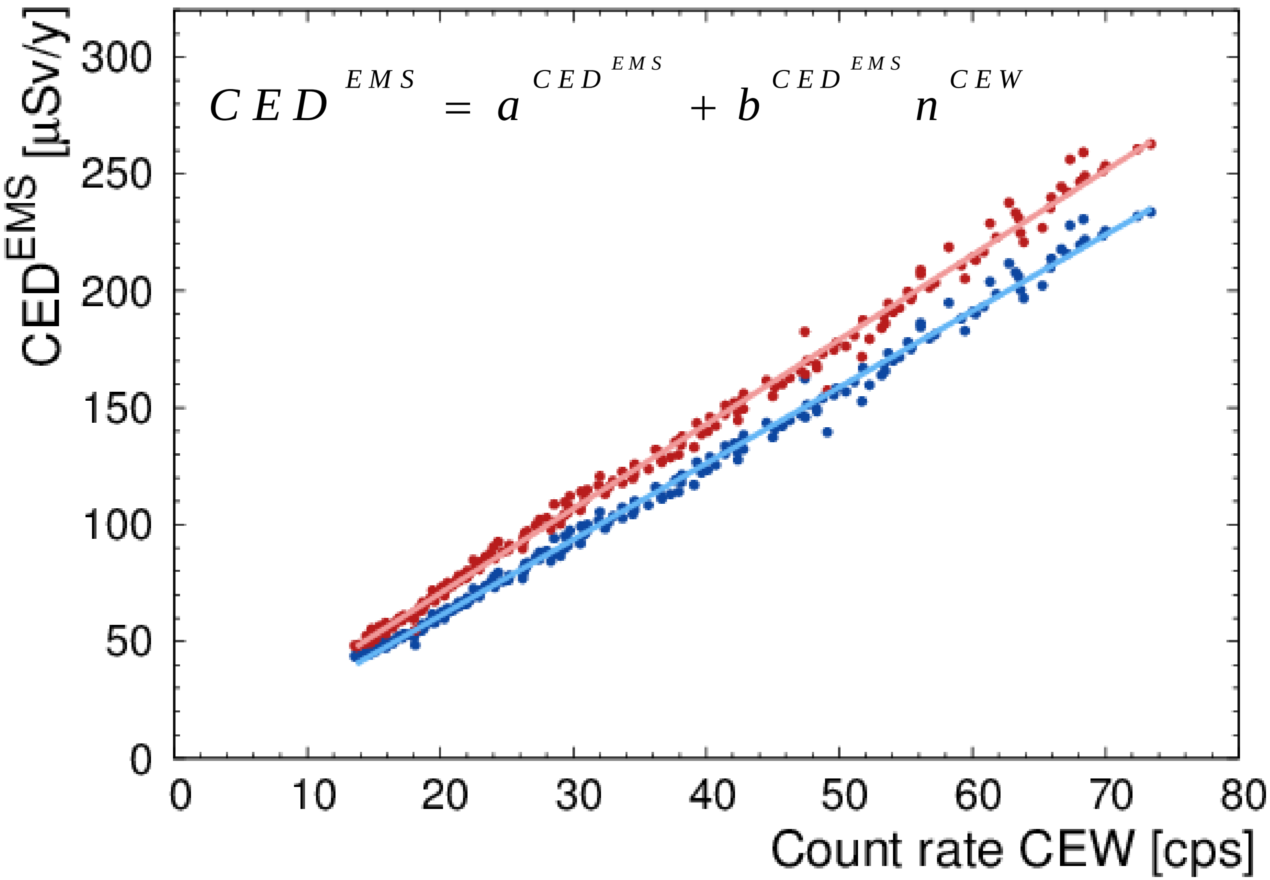

	CED^{EMS}		
	a [μSv/y]	b [μSv/(y·cps)]	r^2
CARI-6P	-4.16 ± 0.59	3.26 ± 0.02	0.996
EXPACS	-1.67 ± 0.67	3.62 ± 0.02	0.996

"CARI-6 program to calculate galactic cosmic radiation" Federal Aviation Administration (2014)
"Analytical model for estimating terrestrial cosmic ray fluxes nearly anytime and anywhere in the world: Extension of PARMA/EXPACS" T. Sato (2015)

Take away highlights

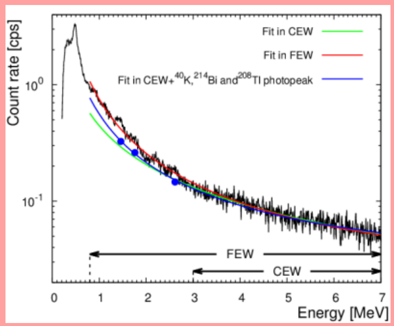

The **cosmic spectral shape** of a measured gamma spectrum was reconstructed by using as additional constraints to the high energy tail the cosmic count rates measured in the ^{40}K,^{214}Bi and ^{208}Tl photopeaks

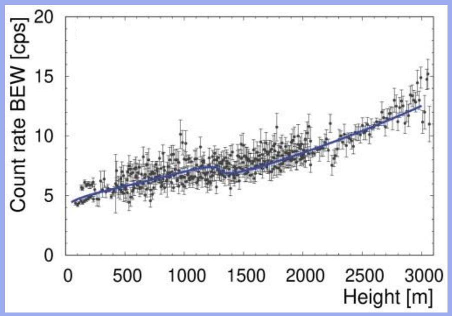

A **new model** accounting for the presence of **atmospheric ^{222}Rn** provides a good reconstruction of the BEW count rate vertical profile, showing the **potential of offshore AGRS measurements in ^{222}Rn monitoring**

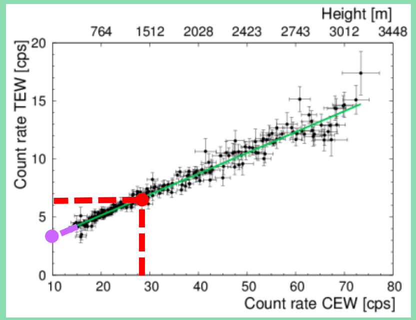

Count rates **linear regression lines** allow for discriminating **cosmic** from **experimental setup radioactivity** background, assessing **background count rates** during AGRS regional surveys and determining **Minimum Detectable Abundances**

Baldoncini M., Albèri M., Bottardi C., Mantovani F., Minty B., Raptis K., Strati V. *Airborne gamma-ray spectroscopy for modeling cosmic radiation and effective dose in the lower atmosphere*. (2017) IEEE Transactions on Geoscience and Remote Sensing

Baldoncini M., Albèri M., Bottardi C., Mantovani F., Minty B., Raptis K., Strati V. *Exploring atmospheric radon with airborne gamma-ray spectroscopy* (2017). Atmospheric Environment